Electronic Supplementary Material (ESI) for Chemical Communications.

Biomimetic artificial cells to model the effect of membrane asymmetry on chemoresistance

Elanna B. Stephenson and Katherine S. Elvira*

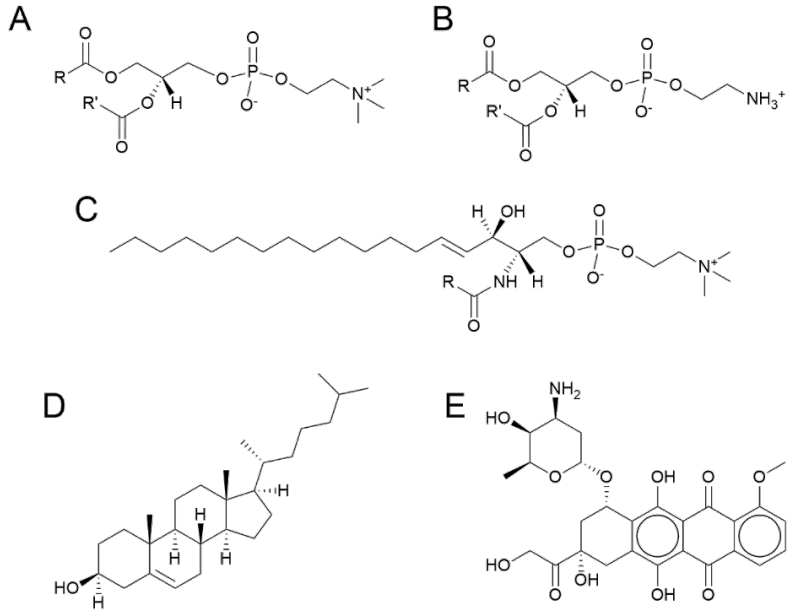

Fig. S1. Chemical structures of compounds used. General structures are shown for phospholipids, with **A)** being PC, **B)** being PE, and **C)** being SM. All of the phospholipids used are naturally derived, meaning that a mixture of several lipid chain lengths are present and substituted at R and R'. **D)** Structure for cholesterol, which is found between the lipid tails in biological membranes and enhances bilayer rigidity **E)** Structure for doxorubicin, a chemotherapy drug.

Bilayer type	Lipid	Outer leaflet (μg/mL)	Inner leaflet (μg/mL)
Asymmetric	PC	2015	830
	PE	830	2015
	SM	240	0
	CHOL	210	210
Blend	PC	1719	1126
	PE	1126	1719
	SM	180	60
	CHOL	210	210
Symmetric	PC	1423	
	PE	1423	
	SM	120	
	CHOL	210	

Table S2. Detailed compositions of lipid formulations. The table shows the exact concentrations of lipids for each leaflet in asymmetric, blend and symmetric DIBs.

3) Materials and methods

Egg l-α-phosphatidylcholine (PC, >99%) and egg sphingomyelin (SM, >99%) were purchased from Avanti Polar Lipids. Egg l-α-phosphatidylethanolamine (PE) was purchased as a reference standard from European Pharmacopoeia. Cholesterol (CHOL, Sigma grade), 4-(2-hydroxyethyl)-1-piperazineethane sulfonic acid (HEPES, BioPerformance certified grade) and KCl (molecular biology grade) were purchased from Sigma. Doxorubicin HCl (>95.0%) was purchased from TCI America.

Aqueous buffer consisted of HEPES (10 mM, pH = 7.4) and KCl (140 mM). To insert DOX into the aqueous droplets, first a 10 mM solution of DOX was prepared by dissolving the doxorubicin HCl in dimethylformamide (DMF). Prior to each experiment, solutions were placed in a vacuum desiccator overnight to remove the DMF, and subsequently reconstituted in buffer at a concentration of 1 mM.

4) Droplet and bilayer size measurements

Relative curvature, bilayer size, and droplet volume were all determined manually in NIS Elements. This process is time consuming, and this in combination with the field of view of the microscope enabling only one droplet pair to be observed at one time, means that throughput of data analysis is lower that the throughput of DIB formation allowed by the microfluidic platform. Automation of image analysis would considerably speed up this process and enable collection of larger data sets.

Channel height ($h_{channel}$, 53 ± 1 μm) was determined by analysing the SU-8 on silicon master wafer with a profilometer (Dektak XT).

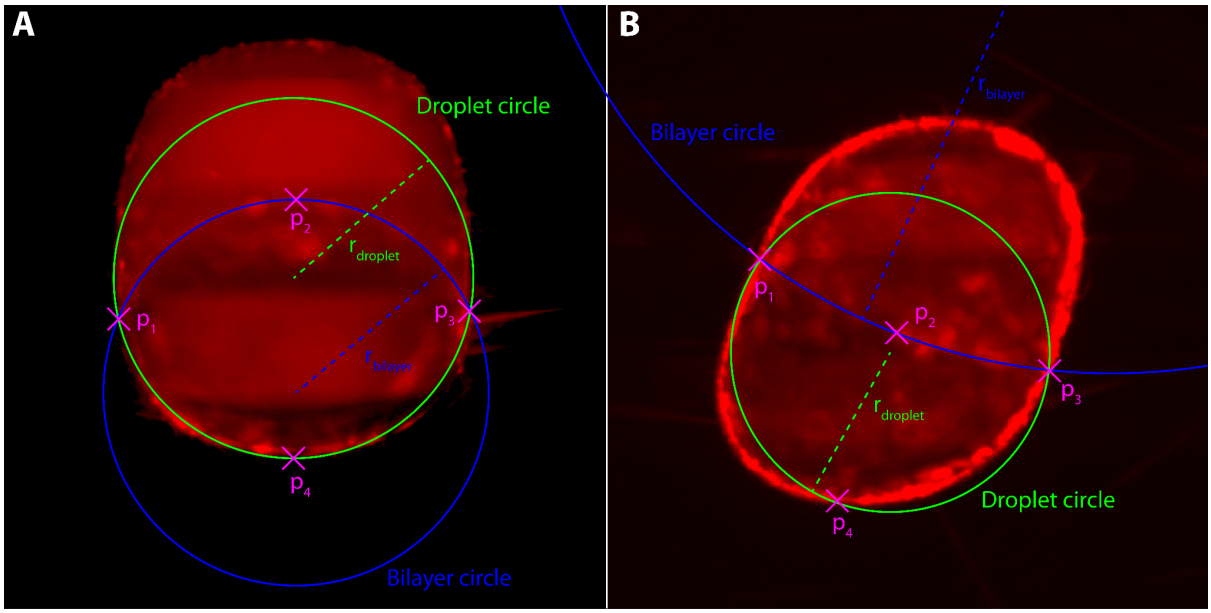

Fig. S4. Relative curvature measurements. For the bilayer radius (blue, $r_{bilayer}$), a circle intersecting 3 points (p_1, p_2, p_3) was drawn, corresponding to the left edge (p_1), center (p_2), and right edge of the bilayer (p_3) respectively. For the droplet radius (green, $r_{droplet}$), a circle intersecting 3 points (p_1, p_4, p_3) was drawn, corresponding to the left intersection with the bilayer (p_1), the edge opposite the bilayer (p_4), and the right intersection with the bilayer respectively (p_3). **A)** Shows an asymmetric bilayer and **B)** shows a symmetric bilayer. The relative curvature was calculated by the following method for each droplet pair at 4 min:

$$Relative\ curvature = \frac{r_{droplet}}{r_{bilayer}}$$

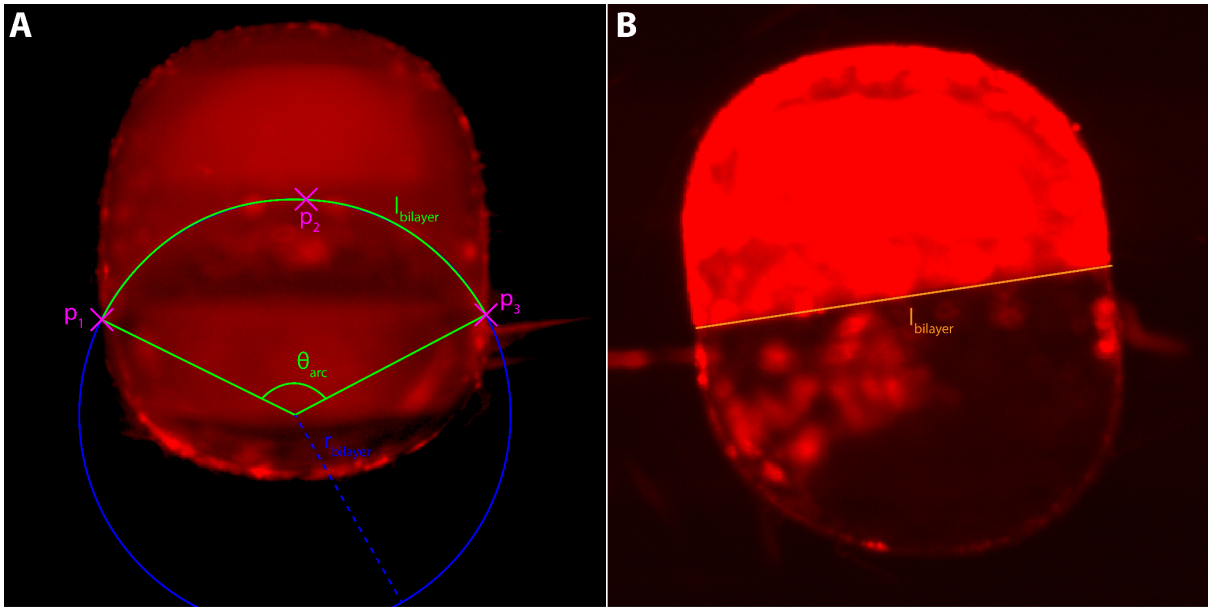

Fig. S5. Bilayer size measurements. A) Method for measuring bilayer length in asymmetric and blend DIBs. Bilayer length was calculated by creating a circle (blue) that intersects 3 points (p_1, p_2, p_3) corresponding to the left edge (p_1), center (p_2), and right edge (p_3) of the bilayer respectively to find the radius ($r_{bilayer}$) of the bilayer. From the center of the circle, the angle (θ_{arc}) between point p_1 to point p_3 was measured. The bilayer's length ($l_{bilayer}$) was then calculated as the length of an arc (green) using: $l_{bilayer} = \frac{2\pi r_{bilayer}\theta_{arc}}{360°}$. **B)** Method for measuring bilayer length (orange, $l_{bilayer}$) in symmetric DIBs. Bilayers were approximately linear, and were therefore measured as a line segment from the left to the right edge of the bilayer. The bilayer area ($A_{bilayer}$) was subsequently calculated from bilayer length ($l_{bilayer}$) obtained by either method as an oval with a height equal to that of the microfluidic device channel ($h_{channel}$): $A_{bilayer} = \pi l_{bilayer} h_{channel}$. Bilayer area was determined at 0 min, 1 min, 6 min, and 11 min, based on the most rapid rate of change in bilayer area occurring during the first minute of each experiment. The bilayer area at time points between these were calculated by linear interpolation.

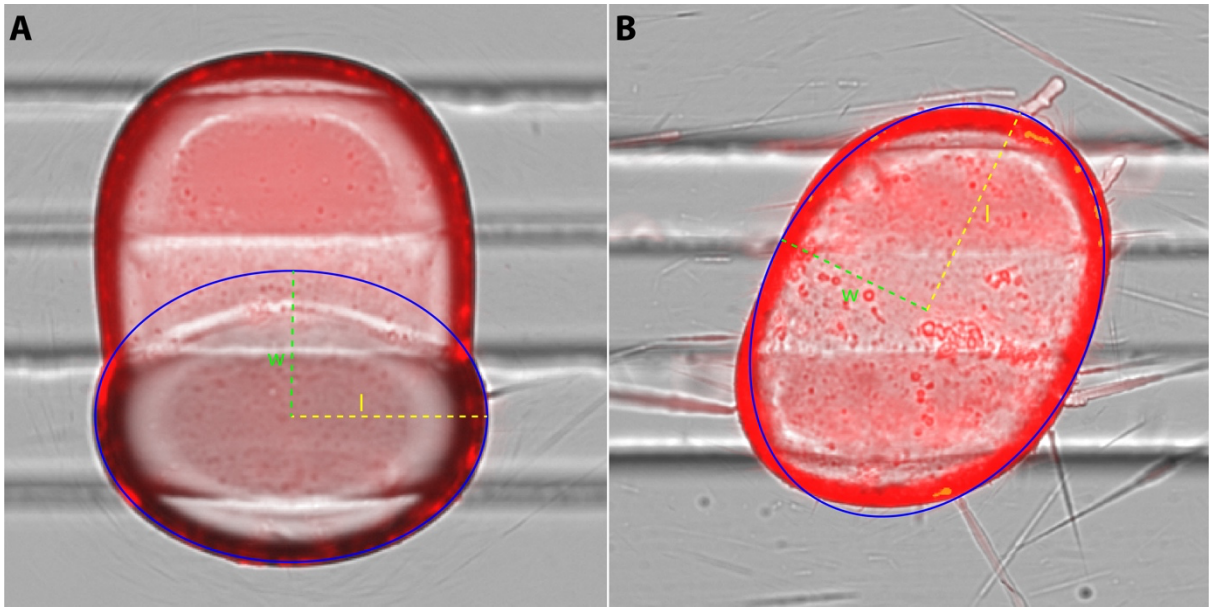

Fig. S6. Droplet volume measurements. A) Method for calculating droplet volume ($V_{droplet}$) in asymmetric and blend DIBs. Acceptor droplet dimensions were measured as an oval (blue) with width w (green) and length l (yellow). The volume was then calculated as an ovoid with a height equal to the channel height ($h_{channel}$) using: $V_{droplet} = \frac{4}{3}\pi lwh_{channel}$. **B)** Method for measuring droplet volume ($V_{droplet}$) in symmetric DIBs. The dimensions of the entire droplet pair were measured with an oval with width w (green) and length l (yellow). The acceptor droplet volume (bottom droplet) was then calculated as half of an ovoid with a height equal to the channel height ($h_{channel}$) using: $V_{droplet} = \frac{2}{3}\pi lwh_{channel}$. Droplet volumes were determined at 1 min, 6 min, and 11 min. The volume at 0 min was treated as the same as at 1 min. The change in volume over the first minute is negligible compared to the measurement error. The droplet volume at time points between those determined were calculated by linear interpolation.

7) Time lapses of bilayer curvature

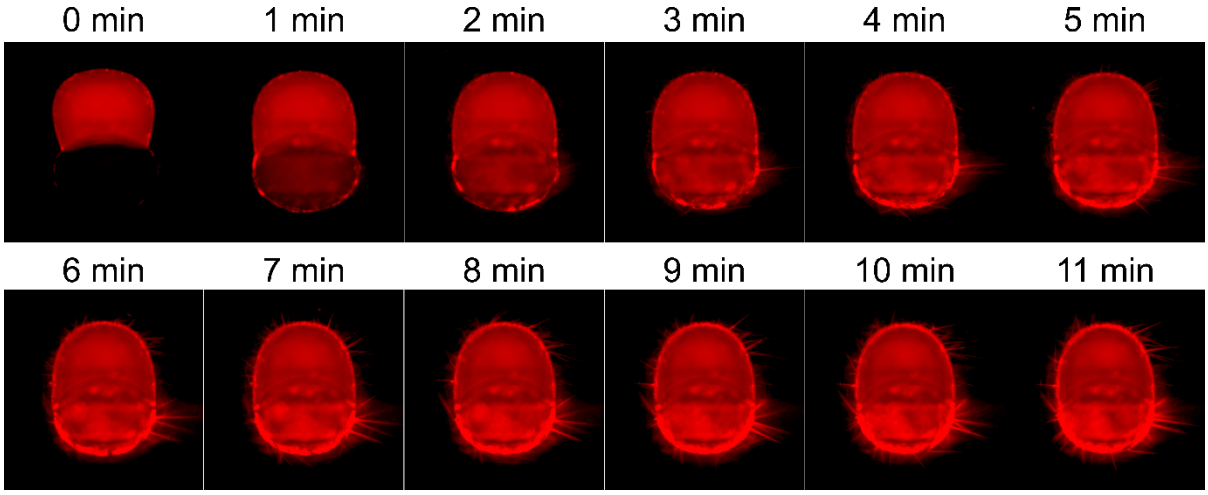

Fig. S7. Evolution of asymmetric bilayer curvature over time. Time lapse of diffusion and bilayer curvature for asymmetric DIBs, as shown in Fig. 3. Bilayer size and curvature change as the bilayer equilibrates over the first 4 min. Following complete bilayer equilibration, bilayer curvature does not change.

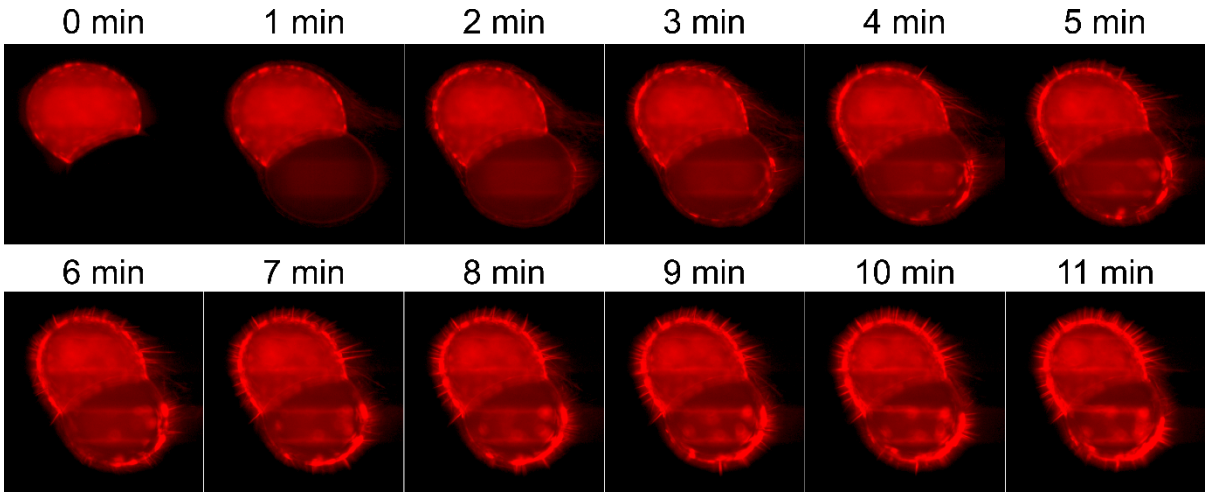

Fig. S8. Evolution of blend bilayer curvature over time. Time lapse of diffusion and bilayer curvature for blend DIBs, as shown in Fig. 3. Bilayer size and curvature change as the bilayer equilibrates over the first 4 min. Following complete bilayer equilibration, bilayer curvature does not change.

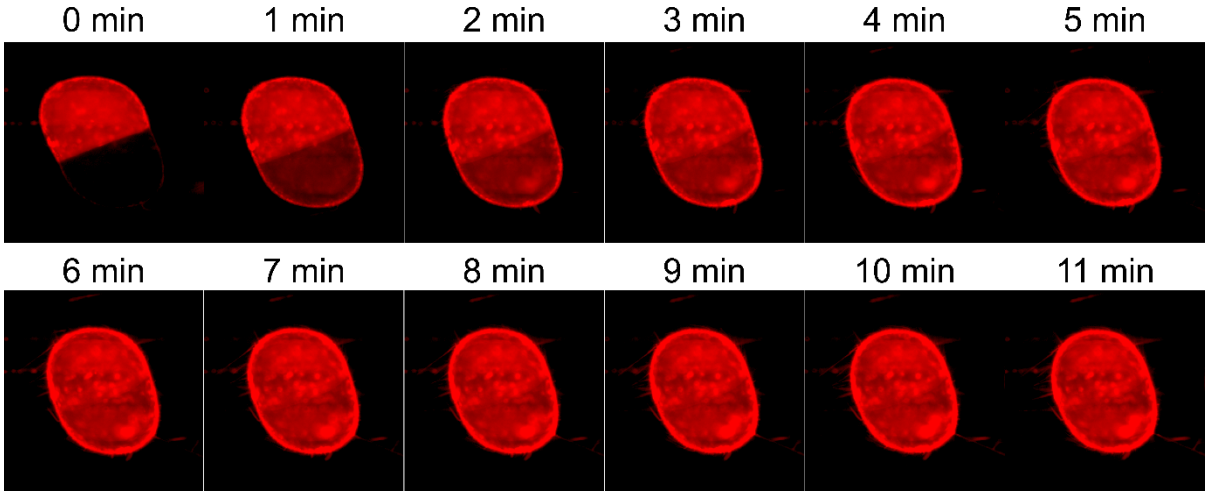

Fig. S9. Evolution of symmetric bilayer curvature over time. Time lapse of diffusion and bilayer curvature for symmetric DIBs, as shown in Fig. 3. Bilayer size and curvature change as the bilayer equilibrates over the first 4 min. Following complete bilayer equilibration, bilayer curvature does not change.

Bilayer type	Outer leaflet interfacial tension (mN/m)	Inner leaflet interfacial tension (mN/m)
Asymmetric	0.789 ± 0.006	15.567 ± 1.012
Blend	0.781 ± 0.001	4.190 ± 2.016
Symmetric	0.785 ± 0.026	

Table S10. Interfacial tension data for lipid solutions. Data was collected on a DataPhysics TBU 90E goniometer by the pendant drop method using two liquid phases. The droplet phase was the buffer solution, and the surrounding phase was the lipid mixture in squalene. Droplets were allowed to equilibrate for 5 min before image capture. Surface tension was calculated from pendant drop images using OpenDrop 3.3.0 (n = 3 in all cases).

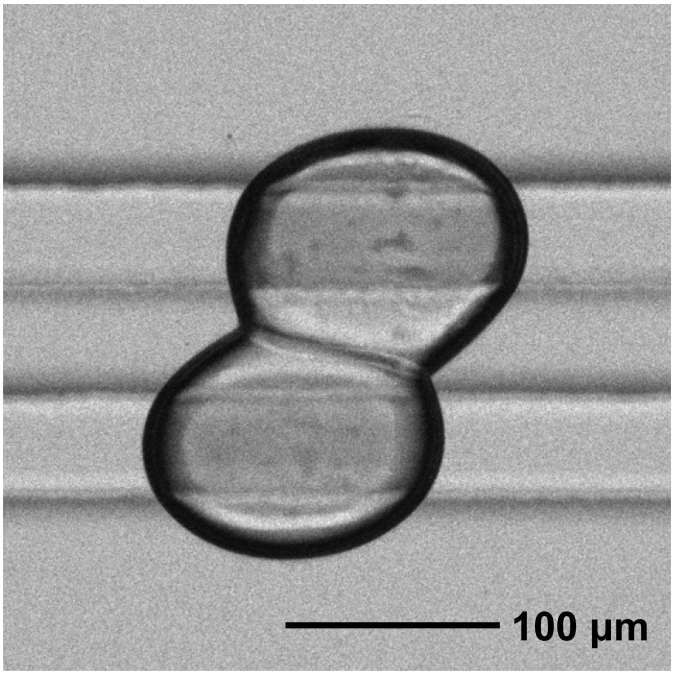

Fig. S11. Effect of SM on bilayer curvature. Representative image showing that an asymmetric distribution of PE (which occupies a conical space) and DOPC (which occupies a cylindrical space) was insufficient to drive formation of bilayers exhibiting curvature. Outer leaflet concentration (top droplet) was 2015 µg/mL DOPC, 830 µg/mL PE and 210 µg/mL CHOL. Inner leaflet concentration (bottom droplet) was 830 µg/mL DOPC, 2015 µg/mL PE and 210 µg/mL CHOL.

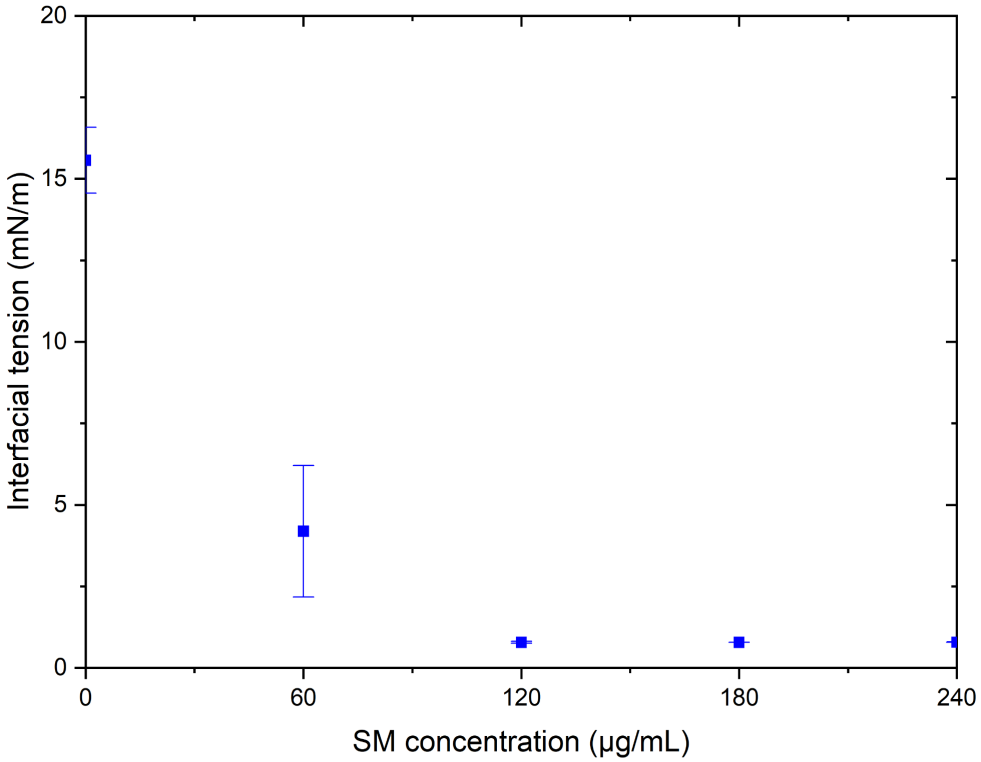

Fig. S12. Relationship between interfacial tension and SM concentration. SM appears to be the largest contributor to the curvature exhibited by asymmetric and blend DIBs, and this appears to be driven by the profound drop in interfacial tension found when using even small amounts of SM. The contribution of PC and PE ratios to the changing interfacial tensions were ignored based on the lack of curvature in asymmetric bilayers seen in Fig. S11.

13) Original fluorescence images

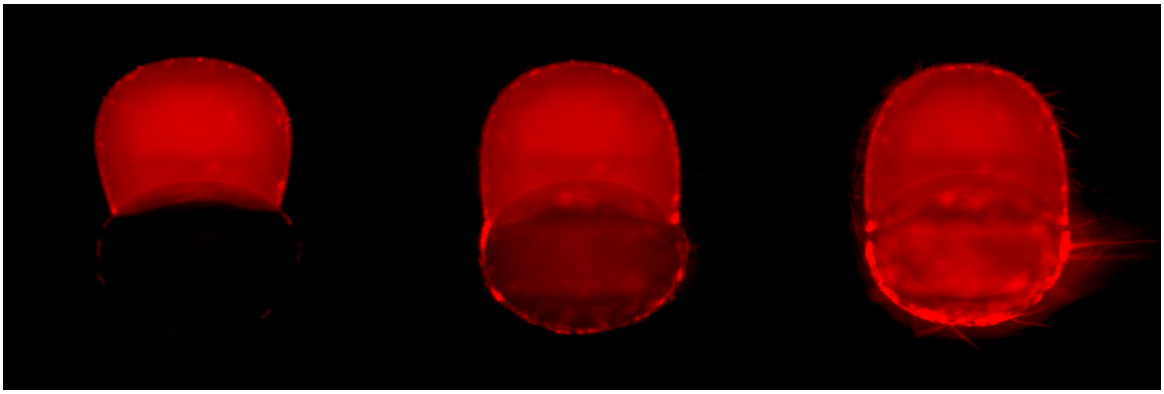

Fig. S13. RGB images for the asymmetric bilayers shown in Fig. 3. In the original figure, a conversion from RGB to CMYK colourspace has been applied. For scale and annotations, see Fig. 3 in the main text. From left to right: 0 min, 1 min, 4 min.

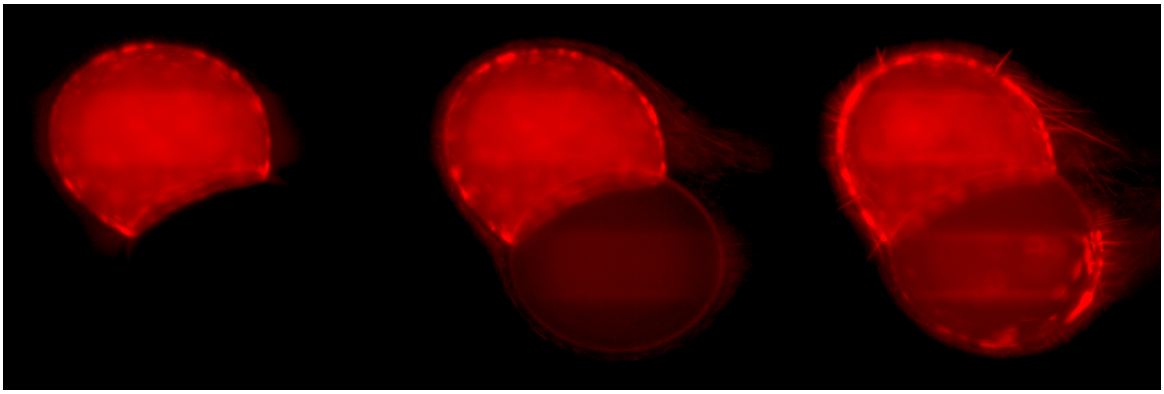

Fig. S14. RGB images for blend bilayers shown in Fig. 3. In the original figure, a conversion from RGB to CMYK colourspace has been applied. For scale and annotations, see Fig. 3 in the main text. From left to right: 0 min, 1 min, 4 min.

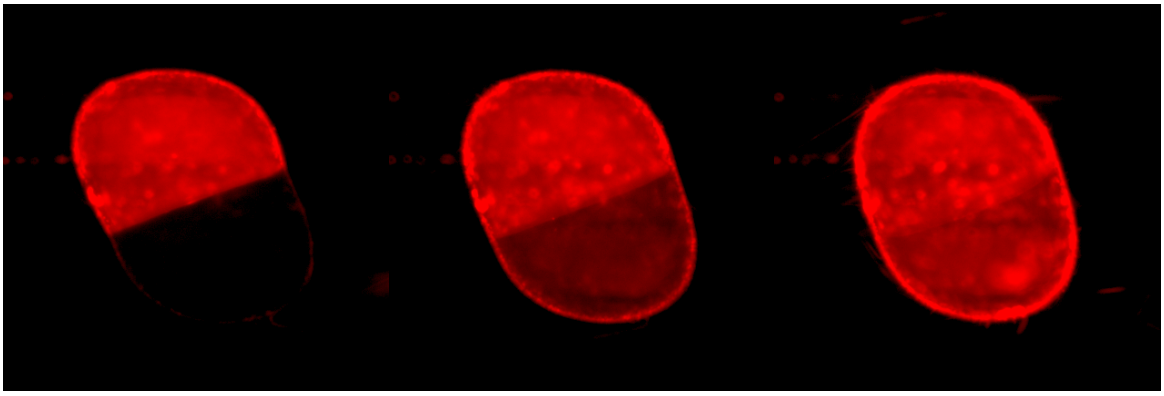

Fig. S15. RGB images for symmetric bilayers shown in Fig. 3. In the original figure, a conversion from RGB to CMYK colourspace has been applied. For scale and annotations, see Fig. 3 in the main text. From left to right: 0 min, 1 min, 4 min.

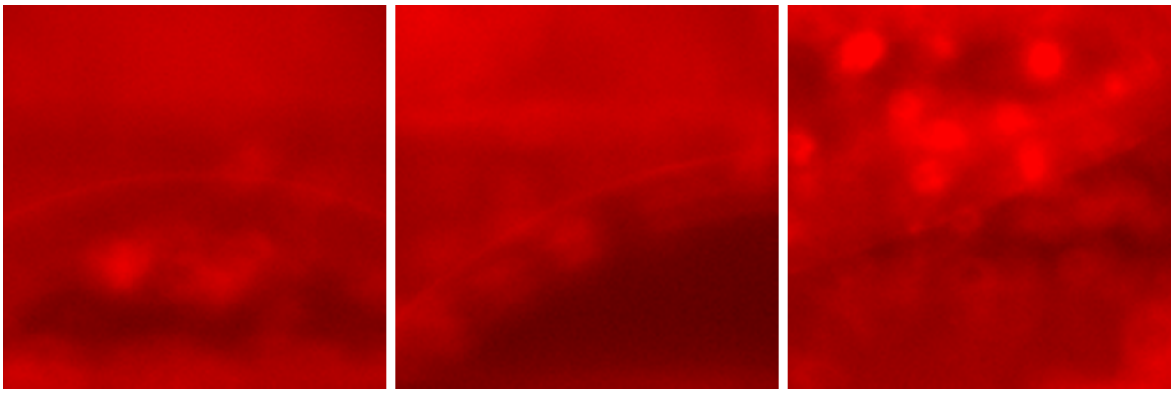

Fig. S16. Original RGB images for expansions shown in Fig. 3. In Fig. 3, a conversion from RGB to CMYK colourspace has been applied. Post processing for visibility was also applied in Fig. 3, with brightness decreased and contrast increased. For scale and annotations, see Fig. 3 in the main text. From left to right: asymmetric, blend, symmetric.

17) Fluorescence intensity measurements and flux calculations

For measurement of fluorescence intensity, a noise-free region of interest was selected on the acceptor droplet. This was preferentially selected on the rail, but if not possible, a point between the rails was selected. The intensity for each time point (I_t) was normalised ($I_{norm,t}$) by subtracting the background (intensity at t = 0, I_0), and scaling by the droplet volume at time t (V_t) over initial droplet volume (V_0) to account for changes in concentration due to evaporation:

$$I_{norm,t} = \frac{(I_t - I_0)V_t}{V_0}$$

Percent absorbed was calculated for the normalized intensity at teach time point ($I_{norm,t}$) as a fraction of the peak normalized intensity ($I_{norm,max}$). Absorbed percentage was converted to concentration (C_t) by multiplying by the estimated concentration at equilibrium (0.5 mM due to the initial donor droplet concentration of 1 mM, and the equivalent donor and acceptor droplet volumes):

$$C_t = \frac{I_{norm,t}}{I_{norm,max}} 0.5\ mM$$

To calculate flux for each time point (J_t), the rate of concentration change from that time (C_t) to the next time point (C_{t+1}) was calculated. This in turn was divided by the bilayer area at that time (A_t) and the size of the time step (Δt):

$$J_t = \frac{C_{t+1} - C_t}{(A_t \Delta t)}$$

A curve was fitted to concatenated flux data from all replicates for each experimental condition (asymmetric, blend, symmetric). The data was fitted to a first order exponential decay in OriginPro 2021 of the form:

$$y = y_0 + A_1 e^{-x/t_1}$$

Where y_0 is the offset from baseline, A_1 is the initial value before offset, x is the time, and t_1 is the mean lifetime. Peak flux, or initial flux (J_{max}) for each experimental condition was calculated from the fitted equation as:

$$J_{max} = y_0 + A_1$$

Calculated flux (J_t) is highly dependent on bilayer size, dependent upon droplet volume ratios from donor to acceptor, and to a lesser extent dependent on volume changes over time. Hence we normalise for this in our data analysis. However, the larger error calculated in P_{app} and curvature for the blend bilayers may be due to the larger degree of variability observed in interfacial tension measurements for the inner leaflet of these blend bilayers (see Table S10). This may be due to improper membrane packing.

18) Acknowledgements

Dr Elvira's position is funded through the Canada Research Chair program and the Michael Smith Foundation for Health Research Scholar program in partnership with the Pacific Alzheimer Research Foundation. Funding for this work was provided through the Natural Sciences and Engineering Research Council of Canada (NSERC) Discovery Grant program, the Canada Foundation for Innovation John R. Evans Leaders Fund (CFI-JELF), the British Columbia Knowledge Development Fund (BCKDF), and the NSERC Research Tools and Instruments program. We would like to thank Dr Ned Djilali for use of his lab space and equipment for carrying out interfacial tension measurements.